New Insights into $\chi^{(3)}$ Measurements: Comparing Nonresonant Second Harmonic Generation and Resonant Sum Frequency Generation at the Silica/Aqueous Electrolyte Interface

Benjamin Rehl, Mokhtar Rashwan, Emma L. DeWalt-Kerian, Tasha A. Jarisz, Akemi M. Darlington, Dennis K. Hore, and Julianne M. Gibbs

March 2019

C: Surfaces, Interfaces, Porous Materials, and Catalysis

New Insights on # Measurements: Comparing Non-Resonant Second Harmonic Generation and Resonant Sum Frequency Generation at the Silica/Aqueous Electrolyte Interface

Benjamin Rehl, Mokhtar Rashwan, Emma L DeWalt-Kerian, Tasha A. Jarisz, Akemi M. Darlington, Dennis Kumar Hore, and Julianne Montfort Gibbs

J. Phys. Chem. C, **Just Accepted Manuscript** • DOI: 10.1021/acs.jpcc.9b01300 • Publication Date (Web): 31 Mar 2019

New Insights on $\chi^{(3)}$ Measurements: Comparing Non-Resonant Second Harmonic Generation and Resonant Sum Frequency Generation at the Silica/Aqueous Electrolyte Interface

Benjamin Rehl,[1] Mokhtar Rashwan,[1] Emma L. DeWalt-Kerian,[1] Tasha A. Jarisz,[2] Akemi M. Darlington,[1] Dennis K. Hore,[2] Julianne M. Gibbs[1,]*

[1]Department of Chemistry, University of Alberta, Edmonton, Alberta T6G 2G2, Canada.

[2]Department of Chemistry, University of Victoria, Victoria, British Columbia V8W 3V6, Canada

ABSTRACT

Historically, different pH dependent behaviour at the mineral oxide/aqueous electrolyte interface has been observed by non-resonant second harmonic generation (SHG) and resonant sum frequency generation (SFG), despite a general understanding that both techniques are dominated by the response of water. Here we compare the two at the silica/aqueous interface at high salt concentration and as a function of pH to shed light on the origins of both measurements. From this comparison and SHG measurements at the silica/air interface, we conclude that SHG originates from the net order of water and the silica substrate, with the latter dominating the observed intensities below pH 6.5. In contrast, SFG is dominated by the higher SF activity, yet lower number density, of waters that contribute in the low wavenumber range, according to molecular dynamic simulations. Furthermore, spectral resolution in SFG of oppositely oriented water populations prevents cancellation of signal making it more difficult to relate SF intensity to the net order of water.

TOC Graphic

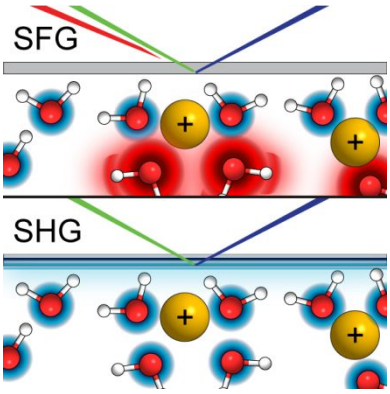

INTRODUCTION

Nonlinear optical techniques (NLO) such as second harmonic generation (SHG) and sum frequency generation (SFG) are powerful methods for studying buried interfaces due to their surface specificity.[1-4] These techniques have been used to enhance understanding of dielectric interfaces such as mineral oxides in contact with water.[5-9] Silica, one such mineral oxide, is one of the most abundant minerals in the Earth's crust and for this reason receives a tremendous amount of attention.[10] As such, non-resonant SHG and vibrational SFG have both been utilized to probe the silica/water interface in the presence of different ions[11-21] and at different pH.[22-28] These studies have revealed that silica is able to affect the order, alignment, and structuring of water molecules due to both electrostatic interactions between the water and charged siloxide sites at the surface that dominate above pH 2 and hydrogen-bonding interactions between water and surface sites.[22-23]

The sensitivity of non-resonant SHG to the presence of surface charges on mineral oxides was first proposed by Eisenthal and co-workers in their seminal paper in 1992.[22] These early studies were conducted at the silica/aqueous electrolyte interface and suggested that the non-resonant second harmonic signal intensity could be explained by the alignment or polarization of water molecules interacting with an interfacial potential (Φ_0) that originated from the charged

silica surface. As such, a new $\chi^{(3)}$ model of SHG was invoked where the electric field oscillating at the second harmonic frequency ($E_{2\omega}$) could be related both to the second-order nonlinear susceptibility $\chi^{(2)}$ and the product of the third-order susceptibility $\chi^{(3)}$ and the interfacial potential Φ_0 according to:

$$E_{\omega_1+\omega_2} \propto \chi^{(2)} E_{\omega_1} E_{\omega_2} + \frac{\kappa}{\sqrt{\kappa^2+(\Delta k_z)^2}} e^{i\varphi} \chi^{(3)} E_{\omega_1} E_{\omega_2} \Phi_0 \quad \text{eq.1}$$

E_{ω_1} and E_{ω_2} are the incident electric fields from the laser source oscillating at frequencies ω_1 and ω_2, respectively, and SHG describes the specific case when $\omega_1 = \omega_2$. Equation 1 also reveals the dependence of the relative phase of $\chi^{(2)}$ and $\chi^{(3)}$ on the salt concentration owing to the relationship between the ionic strength and the Debye length. Here κ is the inverse of the Debye screening length, Δk_z is the inverse of the coherence length, and φ is the $\chi^{(3)}$ phase angle described by $\varphi = \tan^{-1}(\Delta k_z/\kappa)$.[29-35] In non-resonant SHG where neither the incident light frequency nor the SH frequency are on resonance with any electronic or vibrational transition, $\chi^{(2)}$ contains contributions from every molecular species that is non-centrosymmetrically assembled at the silica/water interface. In contrast, $\chi^{(3)}$ describes only the contributions of water based on interactions with the interfacial potential Φ_0.[22]

In the original experiments by Eisenthal and co-workers at the silica/aqueous electrolyte interface the pH was varied from pH 2 to pH 14, and the magnitude of the SHG signal was found to be smallest at pH 2.[22] This low pH corresponded to the expected point of zero charge (pzc) of silica that would result in an interfacial potential of zero. Therefore, the authors proposed that at pH 2 the contribution from the $\chi^{(3)}\Phi_0$ term was zero and the signal stemmed from $\chi^{(2)}$, which was assumed to be independent of potential.[22] Moreover, as the SHG intensity was very low at pH 2, the authors concluded the intrinsic $\chi^{(2)}$ response of the silica/aqueous salt interface was small and

not important in the discussion of the pH-dependent behavior at intermediate and high pH.[22] Increasing the pH from 2 to ~14 led to significant changes in signal intensity (150 fold increase), which the authors attributed to an increase in SH response from water molecules based on interactions between the water and the surface potential as a result of the increasingly negative surface.[22] This argument that pH-dependent trends in SHG intensity originated from the interaction of the surface potential (or surface static field) with water (ie the $\chi^{(3)}$ term) was subsequently used in a significant amount of NLO studies on charged surfaces including silica,[11-13, 24, 36-39] alumina,[40-41] and titania.[42]

The $\chi^{(3)}$ method has also been used to describe another second-order nonlinear optical process, vibrational SFG, for various charged interfaces.[7, 14, 16, 27, 32, 34, 43-47] The expressions for the SFG intensity are very similar as SFG has the same symmetry requirement of a non-centrosymmetric system as non-resonant SHG (equation 1). For vibrational SFG of water, ω_1 corresponds to visible light (λ = 800 nm) and ω_2 is in the infrared such that the IR electric field is on resonance with the O-H stretch of water, thereby reporting specifically on water aligned near the surface.[44-46] Therefore, for vibrational SFG both $\chi^{(2)}$ and $\chi^{(3)}$ originate exclusively from water unlike non-resonant SHG that could theoretically depend on other interfacial species. Nevertheless, non-resonant SHG is generally thought to report mainly on the amount of ordered or polarized water owing to the apparently small contribution from the neutral silica surface (at pH 2) in the original Eisenthal experiments.[7, 43]

Despite the general understanding that both techniques are influenced by the amount of net ordered water, inconsistencies between SHG and SFG have arisen when comparing experiments on silica at high electrolyte concentrations.[14, 23, 48] As mentioned, in the original non-resonant SHG experiments at the silica/water interface $\chi^{(2)}$ was assumed to be small[22] and in all

SHG studies at this interface the pH dependent trend only decreased from high to low pH,[11, 13, 22, 37, 49] while resonant SFG experiments at the same interface exhibited non-monotonic behaviour.[14, 23, 48] If interference between $\chi^{(2)}$ and $\chi^{(3)}\Phi$ is invoked to explain this difference as was applied in studies of interfacial water on alumina,[40-41, 50-51] titania,[42, 52] LB thin films,[53-54] and polymer particles,[55] then SHG intensity should also display non-monotonic pH-dependent behaviour since $\chi^{(2)}$ at the silica/water interface was assumed to be small, yet it does not.

To address the question of whether SHG and SFG both primarily measure water at the silica/water interface, which lies at the heart of the original description of the $\chi^{(3)}$ method, here we compare the non-resonant SHG from the silica/water interface in the presence of 0.5 M NaCl with resonantly enhanced SFG using different polarization combinations. At this high salt concentration, we demonstrate that the pH-dependent trends observed for the two techniques exhibit distinct dissimilarities below ~ pH 6 and postulate three possible causes for the differences observed. These postulates provide a new framework for considering the origin of both non-resonant SHG and resonant SFG and how each measurement relates to the amount of net ordered water at the silica interface.

EXPERIMENTAL SECTION

Laser Assembly – Sum Frequency Generation. Our regeneratively amplified laser (Spectra-Physics, Spitfire Pro, 1kHz, 120fs, 3.3W) is seeded and pumped, respectively, by a Ti-sapphire oscillator (Spectra-Physics, Maitai, 80 MHz) and a Nd:YLF laser (Spectra-Physics, Empower) to produce 800 nm light. This light is passed through a 30/70 beam splitter to direct 2.3 W to pump a noncollinear optical parametric amplifier (TOPAS-C/NDFG, Light Conversion) to generate tunable, broadband IR light (FWHM ~ 120 cm^{-1}). A filter is used to remove any signal and idler

from the OPA from the IR beam which is then passed through a zero-order, tunable half-wave plate (Alphalas), a CaF_2 focusing lens (focal length = 500 mm, Thorlabs), and a polarizer (Thorlabs, LPMIR050-MP2) before reaching the sample. The remaining 1.0 W of 800 nm light from the Spitfire Pro was passed through an air-spaced Fabry-Perot Etalon (TecOptics) to generate narrow picosecond pulses (FWHM ~ 10 cm^{-1}). The visible light is then passed through a polarizer (Thorlabs, LPVIS050-MP2), a zero-order half-wave plate (Thorlabs, λ/2 @ 808 nm), and a BK7 focusing lens (focal length = 500 mm, Thorlabs) before reaching the sample. The visible beam (10-20 μJ/pulse) and IR beam (~14 μJ/pulse) were directed at the sample, an IR-grade fused silica hemisphere (Almaz Optics, IR grade fused quartz (KI), 25.4 mm diameter), at incident angles of 61° and 67° with respect to the surface normal, respectively, and slightly defocused to avoid beam-induced sample damage. These two beams were spatially and temporally overlapped at the sample interface to generate the sum frequency light. The SFG reflection beam was passed through a BK7 recollimating lens (focal length = 400 mm, Thorlabs), a polarizer (Thorlabs), a BK7 focusing lens (focal length = 100 mm, Thorlabs) and a filter (Thorlabs, FES0750) to remove any residual visible light before entering a spectrograph (Acton SP-2556 imaging spectrograph, grating: 1200 grooves/mm and 500 nm blaze wavelength) connected to a thermoelectrically cooled (-75 °C), back-illuminated, charge-coupled device camera (Acton PIXIS 100B CCD digital camera system, 1340 x 100 pixels, 20 μm x 20 μm pixel size, Princeton Instruments).

Laser Assembly – Second Harmonic Generation. The dumped beam from a Ti-Sapphire oscillator (Spectra-Physics, Maitai, 80 MHz, 350 mW average power) was passed through a Glan-Thompson polarizer (B. Halle, UV-grade calcite, PGT 4.10), a half-wave plate (Thorlabs, λ/2 @ 400 – 800 nm) and finally a BK7 focusing lens (Thorlabs, focal length = 100 mm)

directed at our sample at an incident angle of 60°, with respect to the surface normal. The reflected SHG was passed through, a BK7 recollimating lens (Thorlabs, focal length = 100 mm), a filter (Thorlabs, FB400-40, CWL = 400 nm, FWHM = 40 nm) to remove residual 800 nm light, a focusing lens, and a Glan Thompson polarizer (B. Halle) before entering a monochromator (Optometrics, Corp, Mini-Chrom MC1-02) and a photomultiplier tube (Hamamatsu Photonics). The electrical response from the PMT was amplified and counted by a gated photon counter (Stanford Research Systems). The wavelength and quadratic power dependence of the SHG signal was verified prior to each experiment.

Materials. NaCl (99.99%, Alfa Aesar) was used to prepare salt solutions. NaOH (99.99%, Sigma-Aldrich) and HCl (trace metal grade, Fisher Chemical) were used to adjust pH. Sulfuric acid (95.0 – 98.0%, Caledon Laboratories) and hydrogen peroxide (30% w/w in H_2O, Sigma-Aldrich) were mixed in 3:1 or 4:1 ratios and used for piranha cleaning. All materials were used without further purification. Ultrapure deionized water (18.2 MΩ•cm) was used after deionization from a milli-Q-Plus ultrapure water purification system (Millipore). All experiments were performed with freshly prepared solutions.

Sample Preparation. Prior to each experiment, an IR-grade fused silica hemisphere (Almaz Optics, 1-inch diameter) was washed and sonicated (5 min) and washed again in ultrapure water. The hemisphere was immersed in piranha solution (3:1 or 4:1 mixture of H_2SO_4 and H_2O_2, 1 hour) and then rinsed thoroughly with ultrapure water. The hemisphere was then subjected to four rinse/sonication (5 min) cycles with ultrapure water before drying in an oven at 110°C (30 min). NaCl (1.461g) was dissolved in ultrapure water (50 mL) to yield a 500 mM NaCl solution. This salt solution was used to prepare acidic and basic solutions by the addition of HCl and NaOH, respectively, for the adjustment of solution pH. Strongly acidic salt solution was prepared

by dissolving NaCl (0.5844g) in ultrapure water (10 mL) followed by the addition of concentrated HCl (34-37%, 10 mL). Fresh solutions was prepared prior to each experiment. The fused silica hemisphere was removed from the oven and immediately mounted on a custom-built Teflon cell with the flat side of the silica perpendicular to the laser table and in contact with the sample solution. The top of the Teflon cell was exposed to allow for the adjustment of solution pH. A pH probe (Orion™ ROSS Ultra™ Low Maintenance pH/ATC Triode™ combination electrode, 8107UWMMD) was inserted into the exposed opening and used to measure the pH of the solution while adjusting the solution pH and only until a stable pH reading was achieved in order to minimize the effect of probe leakage. The exposed opening was covered with a clean, glass slide while the probe was not inserted into the cell.

SHG Experiments. A freshly cleaned, oven-dried, fused silica hemisphere was mounted to the sample cell and the laser was aligned to the SHG response from the silica/air interface and SHG was collected. The cell was filled with ultrapure water and the sample was allowed to equilibrate for 30 min before collecting SHG. The water was replaced with 500 mM NaCl solution (pH 5.8) and allowed to equilibrate for 15 min before collecting SHG. The pH of the solution was adjusted with acidic or basic solutions made from the freshly prepared stock salt solution. The reported SHG signal was the average intensity of 60 measurements (2 second collection per measurement) after the 5 minutes of equilibration. For very low solution pH, the already acidic solution (pH ~0) was replaced with a strongly acidic salt solution (pH < 0) and the sample was allowed to equilibrate for 30 min before collecting SHG. SHG was collected in p-in, p-out (ppp) and s-in, p-out (pss) polarization combinations. Intensities were corrected for local field effects and normalized to each experiment's silica/500 mM NaCl intensity at initial pH (pH ~5.8). Additional experimental information can be found in the supporting information.

SFG Experiments. A gold-coated fused silica hemisphere (IR-grade) was mounted to the sample cell and used to align the laser and optimize the SFG response before collecting a set of gold reference spectra at ~2900 cm^{-1}, ~3000 cm^{-1}, ~3100 cm^{-1}, ~3200 cm^{-1}, ~3300 cm^{-1}, and ~3400 cm^{-1}. These six frequencies were used to measure SFG at all interfaces and solution pH values. Measured wavenumbers were calibrated through the use of a polysterene reference by passing the IR beam through a polystyrene film, collecting a reference spectrum from the gold/air interface, and comparing the measured SF wavenumbers to the known polystyrene aromatic C-H absorptions at 3026 cm^{-1}, 3059 cm^{-1}, and 3081 cm^{-1}. The gold-coated hemisphere was then replaced with a freshly cleaned, oven-dried, fused silica hemisphere and SFG from the silica/air interface was collected. The remainder of the experiment was carried out in the same manner as SHG following filling the cell with ultrapure water. SFG was collected in ppp, pss and ssp polarization combinations (for example pss denotes p-polarized sum frequency light, s-polarized visible light, and s-polarized IR light, respectively). Sample spectra were acquired for 30s for ppp and 120s for ssp and pss polarization combinations, while gold reference spectra were collected over 1s acquisition times. Background spectra were collected by blocking the IR beam before reaching the sample which were then subtracted from the raw gold reference and sample spectra. The background corrected spectra from the sample were then divided by the background corrected gold reference spectra and plotted against the IR wavenumbers used. These processed spectra were then integrated from 2850 to 3550 cm^{-1} and normalized to the integrated value at initial pH (pH ~5.8). A set of high and low pH titration spectra were then normalized to the maximum intensity at high pH. Data were analyzed using the software Igor Pro 7.05.

Molecular simulations. As we are interested in evaluating the relative population of 3200 cm^{-1} and 3400 cm^{-1} intensity in the SFG spectra, we have performed molecular dynamics simulations of water next to an uncharged hydrophilic interface. A 3.945 nm × 3.796 nm surface was created from a base layer of 10 OPLS/AA methylene united atoms in a hexagonal array (a = 0.438 nm, c = 0.160 nm lattice constants) terminated with an OH group oriented 71.5º from the normal with random azimuth. 100% of the surface sites have an OH group, resulting in a hydroxyl density of 0.0415 nm^{-2}. We have taken care to equilibrate a large enough system to ensure a bulk water density of 1.0 g/mL in the center of our 10 nm deep box. The resulting density profile and distance-dependent order parameters show significant structuring up to approximately 4 Å into the aqueous phase.[56] 1980 SPC/E water molecules were then added to a total box depth of 10 nm. GROMACS 4.5.5 was used to run the simulations, employing Berendsen temperature coupling at 300 K, three-dimensional periodic boundary conditions, van der Waals interactions cut at 1.2 nm, PME electrostatic interactions with a real-space equivalent cut-off of 1.2 nm. Following energy minimization and equilibration, one out of every 50 frames were sampled from a 10 million frame trajectory with a timestep of 1 fs to yield 200 000 snapshots for analysis, recording Cartesian coordinate and force data. Following the instantaneous normal mode approach developed by Morita and Hynes, the net force along each OH bond was determined. This was then mapped onto a result parameterized from previous electronic structure calculations[57] to arrive at the uncoupled OH stretching frequencies of the hydrogen-bonding environment specific to each OH oscillator. The two OH frequencies were then coupled to arrive at the low- and high-energy eigenmodes, analogous to the symmetric and antisymmetic modes in gas-phase spectra. We then consider any species whose low energy mode fell into the 3150–3250 cm^{-1} window to be associated with the 3200 cm^{-1} intensity, and species in the 3350–3450 cm^{-1} region as

belonging to the 3400 cm^{-1} peak. This enabled comparison of populations in these two distinct spectral regions, irrespective of the associated hyperpolarizability values or the contributing molecular orientations.

RESULTS AND DISCUSSION

Figure 1A illustrates the *ssp*-SFG spectra (s-polarized SFG, s-polarized E_{ω_1} (E_{VIS}), p-polarized E_{ω_2} (E_{IR})) at the silica/aqueous sodium chloride interface (500 mM) from pH 0 that lies below the point of zero charge of silica, to pH 12 where silica is very negatively charged. At this high ionic strength we note two specific effects at the silica/aqueous electrolyte interface: salt addition is known to induce changes to the surface charge density of silica,[24, 58-59] and screening of surface charges by sodium cations results in a short Debye length.[60] Given the concentration of NaCl used in this study, the total ionic strength change due to the pH adjustments was small (2% increase from initial pH to either pH 2 or 12) relative to the initial concentration. We also note at this high ionic strength, which corresponds to a short Debye length (~4 Å at 500 mM ionic strength[61]), the phase mismatch term between $\chi^{(2)}$ and $\chi^{(3)}$ shown in equation 1 is small (ie. $\frac{\kappa}{\sqrt{\kappa^2+(\Delta k_z)^2}} = 0.99997$) and the $\chi^{(3)}$ phase angle, φ, is close to zero degrees $(0.4°)$. Therefore we assumed the phase mismatch factor was equal to 1 and φ was equal to $0°$ for the current analysis. This approximation is consistent with previous vibrational SFG studies that suggested that the phase factor could be ignored for salt concentrations greater than 0.4 M,[62] while for SHG the phase factor only became critical below 1 – 10 mM ionic strength.[34] In order to more closely analyze the pH-dependent trends of the silica/water interface studied by SFG and compare them with non-resonant SHG, the integrated sum frequency signal from 2850 – 3550 cm^{-1} and the second harmonic signal are compared (Figure 1B). From the integrated

intensities of the SFG we see that the total SF signal exhibited a local minimum at ~ pH 6, consistent with our earlier work,[48] and a local maximum at ~ pH 2, which is the expected point of zero charge.

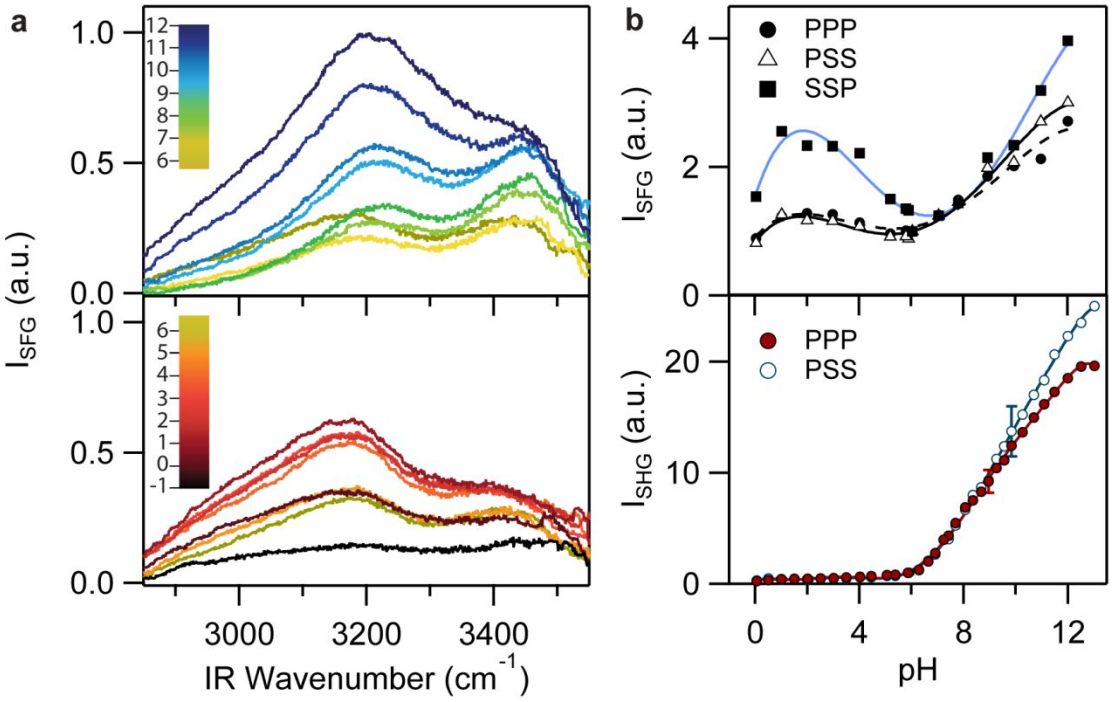

Figure 1. a) ssp-SFG spectra from 2850 – 3550 cm^{-1} measured at the silica/water interface at 500 mM NaCl over a pH range of 5.8 to 12 (top panel) and 5.8 to below 0 (bottom panel). SFG spectra are corrected for local field effects and normalized to maximum intensity at high pH. b) Integrated SFG intensities at the ssp, pss, and ppp polarization combinations (top) and the SHG intensity at the p-in/p-out (ppp) and s-in/p-out (pss) polarization combinations over the pH range studied. Integrated SFG intensities and SHG intensities are normalized to their values at pH 6. Smooth lines are guides for the eye.

In previous SFG experiments, the non-monotonic trend in water response with varying pH was associated with a flip in water that occurred approximately at the pH where the minimum

in SF intensity was observed.[26, 48, 50-52] In our previous work, we had also noted that the low wavenumber region that dominated the ssp and ppp-SFG spectra exhibited the non-monotonic behaviour while the high wavenumber region did not but decreased systematically with decreasing pH.[48] Our analysis and supporting simulations found that the waters contributing to the low wavenumber range flipped upon decreasing the pH from 12 to 2, whereas those contributing to high wavenumber range did not. In support of this analysis, a change in sign of the imaginary part of the SFG response ($Im\chi^{(2)}$) has been observed only for the low wavenumber region at the silica/water interface upon passing from high to low pH, consistent with flipping of only those corresponding water molecules.[26, 63]

However, these non-monotonic intensity trends were never observed for the SHG intensities (Figure 1B), which simply decreased in magnitude from high to low pH for both polarization combinations. This general decrease in SHG with decreasing pH is consistent with our previous work[11, 13] and that of Eisenthal,[22] yet a distinct bimodal feature (double sigmoid) was formerly observed in these surface titrations. We performed systematic experiments to identify why this was absent in our new observations (provided in the supporting information). The difference in shape of the SHG pH titration in these experiments appears to arise from the use of IR-grade silica instead of UV-grade silica, as well as the influence of different starting pH owing to hysteresis, which is significant in pH titrations for silica.[9, 49] Nevertheless, for this study, direct comparisons between SHG and SFG can be made as the same samples were used as well as the same experimental procedures.

We propose three plausible explanations for the observed differences in the pH dependence of the SFG and SHG intensities.

1. Resonant SFG contains contributions from only water whereas non-resonant SHG contains significant contributions from both water and silica. To determine whether silica contributed significantly to the non-resonant SHG, the second harmonic signal was measured at the silica/air interface and compared with that at the silica/water interface after accounting for the local field effects of the pss polarization combination in both experiments. From this comparison, it is seen that the second harmonic electric field from the silica/air interface equals that of the silica/water interface at pH ~6.5 (Figure 2). Below this pH, we observe greater SHG from the silica/air interface than from the silica/aqueous interface. We cannot state that the $\chi^{(2)}$ of silica in contact with water would be precisely the same as that observed in air; nevertheless it would seem unlikely that such a large signal vanishes entirely upon interaction with water.

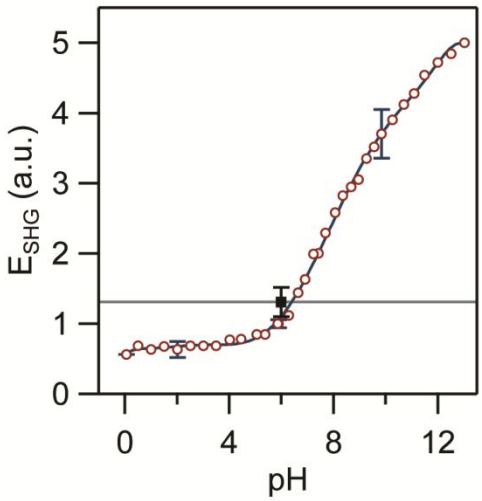

Figure 2. Comparison of pss-SHG electric field at the silica/water interface (500 mM NaCl, circles) to the pss-SHG electric field at the silica/air interface (square and horizontal line). Error bars represent the standard deviation between multiple experiments. The smooth line is a guide for the eye.

Recently, Bonn and coworkers suggested that the SHG signal from the air/membrane monolayer/aqueous interface arose from a convolution of contributions from the water and the membrane surface, with an additional component being hyper-Rayleigh scattering.[54] For a composition of the mixed monolayer that was neutral, the water response was very small according to phase-sensitive ssp-SFG experiments, yet the SHG intensity was substantial. Furthermore, the imaginary component of the SFG response of water changed sign upon transitioning from a negatively charged membrane to a positively charged membrane. Therefore, the authors proposed that $\chi^{(2)}$ stemmed from the SHG response of the membrane which was significant and remained constant with pH while the $\chi^{(3)}\Phi$ term stemmed from the amount of water, which could be determined independently by integrating the ssp-SFG imaginary spectra. At the positively charged interface, $\chi^{(2)}$ from the substrate interfered destructively with the water response manifested in $\chi^{(3)}\Phi$. This destructive interference between the $\chi^{(2)}$ and $\chi^{(3)}\Phi$ terms has also been proposed for SHG measurements at titania[42] and alumina[40-41] surfaces at pH values below the pzc.

To test this SHG model for the silica/aqueous interface where $\chi^{(2)}$ stemmed from the substrate and the $\chi^{(3)}\Phi$ response could be approximated by the integrated ssp-SFG response of water, we first determined the SHG response stemming exclusively from the water. This was achieved by subtracting the square root of the local field corrected SHG intensity at the silica/air interface from the square root of the local-field corrected SHG intensity at the silica/aqueous interface. This analysis was based on our approximation of the $\chi^{(3)}$ phase angle to be 0° (or 180°) among all contributing terms (ie. $\chi^{(2)}_{silica}, \chi^{(2)}_{H_2O}$, and $\chi^{(3)}_{H_2O}\Phi_0$). Moreover we assumed that the silica response was unchanging with varying pH and equivalent to what was measured at the silica/air interface. The resulting SH water response should be proportional to $\left|\chi^{(2)}_{H_2O} + \chi^{(3)}_{H_2O}\Phi_0\right|$

(Figure 3A). We also include the square root of the integrated SFG intensity after local field corrections, which provides an estimate of the SF water response as it does not take into consideration the non-resonant contribution or interfering modes. To determine how much the intensities varied for the two different measurements, we also squared the SH water response value resulting in the SHG intensity that should stem from water. This value is compared this with the integrated SFG intensity after local field corrections for the ssp and pss polarization combinations (Figure 3B).

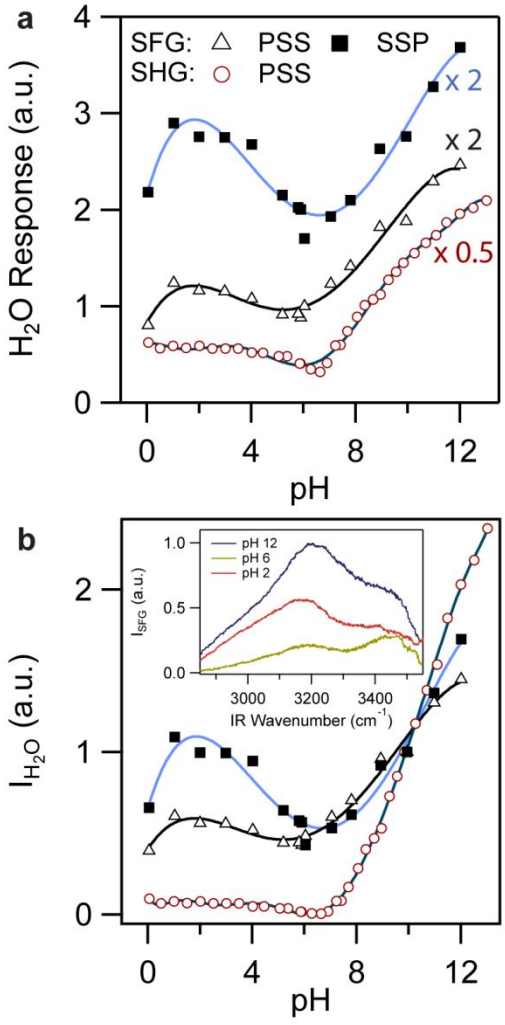

Figure 3. a) The water response proportional to $\left|\chi^{(2)}_{H_2O} + \chi^{(3)}_{H_2O}\Phi_0\right|$ calculated from SHG and integrated SFG. Data are offset and multiplied for clarity. b) The integrated SFG intensities compared to the square of the second harmonic water response. Intensities are normalized to their values at pH 10. (inset: SFG spectra at the silica/aqueous sodium chloride interface at pH 12, 6, and 2. Smooth lines are guides for the eye).

Firstly, the minimum in the SHG response from water occurred at a pH near the pH were the minimum in the SFG response of water was observed (Figure 3A). This observation supports the Bonn model for interpreting SHG, where the $\chi^{(2)}$ stemmed from the substrate and the $\chi^{(3)}\Phi$ term was captured by the integrated ssp-SFG imaginary spectra of water. Next we compared the minimum in intensity stemming from water for SHG and SFG with both measurements normalized to their respective values at pH 10. For SHG, the water response was zero at the minimum (~ pH 7), which is consistent with the SHG from the silica/air interface being greater in magnitude than that measured at lower pH for the silica/aqueous interface (Figure 3B). Yet for the SFG, we observed a significant amount of SF response at this pH compared to what was observed at higher and lower pH (Figure 3B). Furthermore, the SFG intensity spectrum for the silica/aqueous electrolyte interface at pH 6 exhibited pronounced peaks at 3200 cm^{-1} and 3400 cm^{-1}, suggesting a significant amount of ordered water at this pH (Figure 3B, inset). Additionally, the increase in water intensity for ssp-SFG in the low pH region suggested that the amount of aligned water at ~ pH 2 was approximately equal to that observed at pH 10 (Figure 3B). In contrast, the SHG water intensity at pH 2 was twelve times lower than that at pH 10 indicating that the amount of aligned water contributing to the SHG differed from that contributing to the ssp-SFG. These observations suggested that the differences in SHG and SFG

were not completely captured by the SHG from the silica alone and the integrated ssp-SFG spectra, which leads to the second proposed difference in the two measurements.

2. SHG measures the orientational average of all water molecules leading to cancellation of some aligned populations, whereas SFG can spectrally resolve such populations. The trend observed by SHG may also be explained by interference between the signals originating from the water populations that primarily contribute to the 3200 cm^{-1} and 3400 cm^{-1} modes in SFG (Figure 4). As previously mentioned, phase-sensitive measurements at the silica/water and silica/HOD interface as a function of pH and at low salt concentration found that the low wavenumber region exhibited a change in sign of $Im(\chi^{(2)}_{eff})$ upon decreasing from pH 12 to 7 to 2, while the high wavenumber region did not.[26, 63] Furthermore, at high pH the $Im(\chi^{(2)}_{eff})$ spectrum was entirely positive whereas at low pH, the low wavenumber region was negative while the high wavenumber region remained positive. We also proposed a flip in orientation of only the water contributing to the low wavenumber region based on our simulations of the SFG response of a hydrophilic surface/water interface and the observed pH dependent trends at both high and low wavenumbers.[48] Additionally, the phase-sensitive measurements on silica revealed that at low pH the water populations were opposite in orientation, which for our experimental conditions should occur below pH 6.5, where the minimum in SFG intensity was observed (Figure 4).

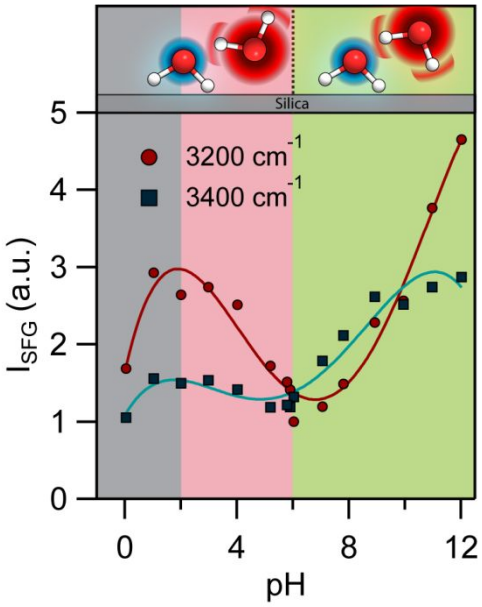

Figure 4. Intensities of ssp-SFG at a) 3185 cm^{-1} and b) 3455 cm^{-1} normalized to the intensity at 3185 cm^{-1} measured at pH 6. Green and red shading indicate possible constructive and destructive interference between water populations, respectively. Smooth lines are guides for the eye. Top: Illustration of flipping water molecules contributing to the low wavenumber region.

As SHG measures the orientational average of all water molecules, cancellation between populations that are oriented in opposite directions could result in lower SHG, unlike SFG which separates populations based on their different resonant OH vibrations. Consequently, even if water assemblies were oppositely oriented they could contribute to the SFG intensity if the assemblies had significant differences in their resonant frequencies, which would be the case for the waters contributing at low (3200 cm^{-1}) and high (3400 cm^{-1}) wavenumber. This scenario would explain why the SHG was much lower in intensity below pH 6.5 than the integrated SFG, as the cancellation of oppositely oriented water populations should occur for the former at lower pH.

3. SFG is weighted by the intrinsic resonant hyperpolarizabilities of water whereas SHG is sensitive to the total number of aligned water molecules in each population. When integrating the SFG to approximate the amount of ordered water, another underlying assumption is that the orientationally averaged resonant molecular hyperpolarizabilities of the modes contributing at 3200 cm^{-1} ($\langle\beta_{3200}\rangle$) and at 3400 cm^{-1} ($\langle\beta_{3400}\rangle$) are roughly equivalent. Accordingly, the intensity at low and high wavenumber would reflect the number of aligned water.

To determine whether the SFG activity of waters contributing at low and high wavenumber were roughly equivalent on a per molecule basis, we performed MD simulations of the average molecular hyperpolarizabilities of water in contact with a polar surface and determined the average hyperpolarizability at 3200 cm^{-1} and 3400 cm^{-1}. Although there have been simulations with explicit silica surfaces,[64-66] we have opted for our simplified model hydrophilic surface described in the experimental section as we have extensively compared its resulting interfacial water structure and generated model SFG spectra from this system[48, 56, 67] in comparison to experimental homodyne and phase-resolved spectra.[26, 33, 63, 68-69] In Figure 5A, C and E, we report the log of the ratio of these 3200 cm^{-1} and 3400 cm^{-1} hyperpolarizability per molecule values as a function of twist and tilt angle for ppp, ssp and pss polarization combinations, respectively. Although the log ratio values vary considerably depending on the twist and tilt angle, we see that overall the vast majority of twist and tilt angles lead to log ratio values greater than 0 for the ssp and ppp polarization combinations (Figure 5B, and F, respectively), which corresponds to $\langle\beta_{3200}\rangle$ greater than $\langle\beta_{3400}\rangle$. This indicates that the water contributing at 3200 cm^{-1} is intrinsically more SFG active at most twist and tilt angles for the ssp and ppp spectra. Moreover, the simulations of the ssp-SFG found that the 3400 cm^{-1} region contained a greater number of contributing oscillators than the 3200 cm^{-1} region by a factor of

1.8, despite the greater intensity observed at 3200 cm^{-1} and 3400 cm^{-1} in the simulations[56] (which is consistent with the experimental results observed at low pH and low salt concentration[14, 25-26, 48, 52, 63]). These simulations suggest that using the integrated ssp or ppp-SFG spectra to understand the amount of aligned water in the system exaggerates the contributions from water contributing to the low wavenumber region, which are lower in number but greater in SFG activity. In contrast, as SHG is a non-resonant measurement in our experimental configuration, to a first approximation the non-resonant hyperpolarizabilities behind these two resonant features should be the same (in other words we are assuming changes in hydrogen bonding does not substantially change the non-resonant hyperpolarizability of water). As such, SHG should be most sensitive to the total number of water molecules that are aligned by the field unlike SFG, which spectrally resolves the different water populations and is sensitive to their intrinsic SF activity.

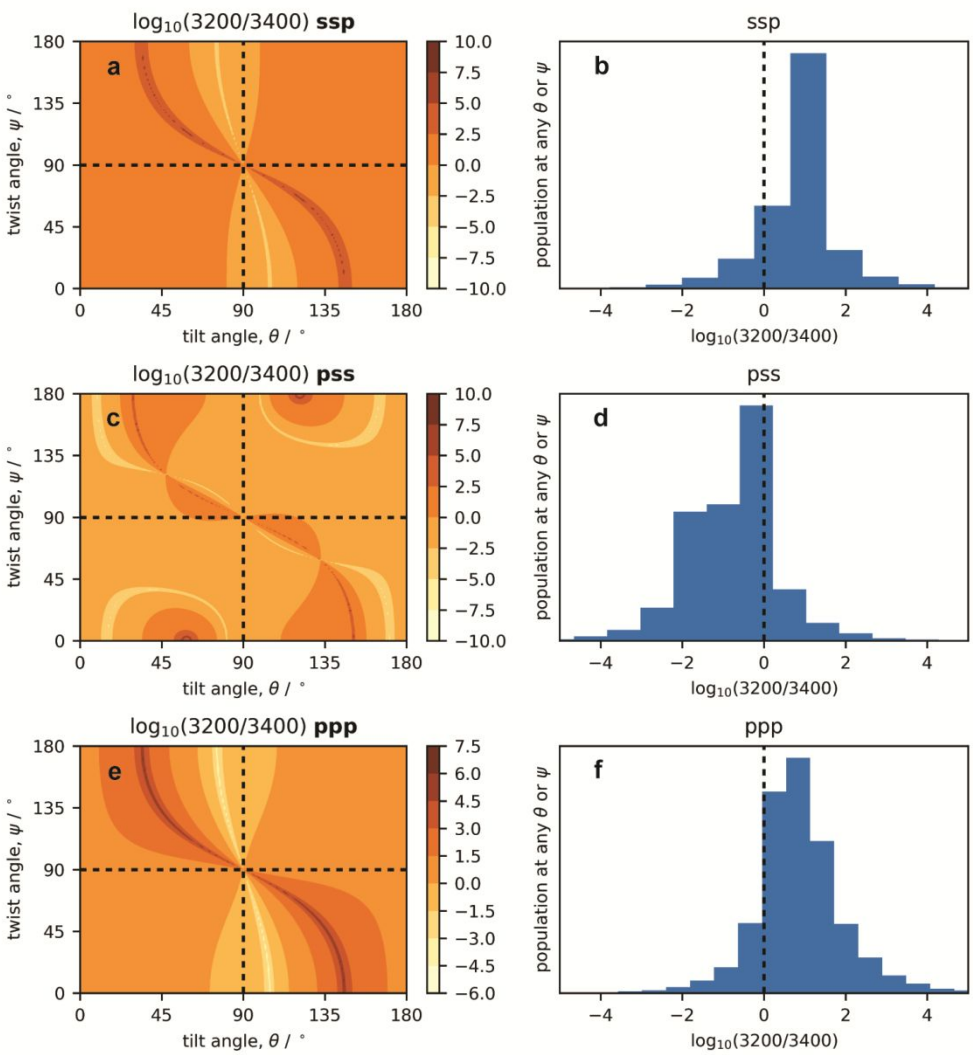

Figure 5. Log ratios of β_{3200} and β_{3400} at all possible twist and tilt angles calculated for the A) ssp, C) pss and E) ppp polarization combinations. Histograms of the frequency that each log ratio value occurred in the corresponding twist and tilt maps are shown for the B) ssp, D) pss and F) ppp polarization combinations.

CONCLUSIONS

In summary, the pH dependence of the silica/water interface measured by non-resonant SHG and vibrational SFG exhibit substantial differences. We attribute these differences to three possible origins: 1) the underlying silica substrate contributes significantly to the SH signal but not SFG owing to resonant enhancement of the water for the latter; 2) destructive interference arises in SHG from different populations of oriented water at lower pH that are spectrally resolved in SFG and therefore do not lead to cancellation of signal; and 3) SHG is sensitive to the number density of aligned water whereas SFG is strongly influenced by the different intrinsic SFG activities of water populations experiencing different chemical environments. None of these possibilities are mutually exclusive and several may contribute to the observed differences between measurements performed using SHG and SFG spectroscopy. Nevertheless, from this investigation we propose that care must be taken in using the integrated ssp-SFG or ppp-SFG since the amount of net ordered water in the system contributing to the high wavenumber region of the ssp and ppp-SFG water spectra, which has lower intensity, actually contains the greatest number of aligned water molecules. Furthermore, spectral resolution of SFG allows water populations of opposite orientation to contribute substantial intensity making it difficult to relate the SFG intensity to the net amount of ordered water. With respect to interpreting SHG results, attention must also be paid when interpreting the SHG intensity at the solid/liquid interface as directly proportional to the net amount of aligned water. Specifically, the $\chi^{(2)}$ contribution from the substrate must be known; if the observed signal intensity is lower than that observed for the bare substrate, this suggests destructive interference is occurring between the signal arising from the net alignment of water and that of the substrate. Accordingly, a decreasing signal intensity could be indicative of *more* rather than less aligned water, owing to such destructive interference. In particular, for the mineral oxide/water interface, destructive interference between the substrate

response and that of the net aligned water should be considered when the SHG intensity becomes very small, which for silica occurs at high salt concentration and lower pH.

ASSOCIATED CONTENT

Supporting Information.

All ppp, ssp and pss SFG spectra shown with and without correction for local field effects. A description of the local field corrections including refractive indices used. The SHG data from our systematic investigation of the effect of experimental parameters on our pH-dependent SHG intensities and additional SHG experimental information. The following files are available free of charge via the Internet at https://pubs.acs.org.

AUTHOR INFORMATION

Corresponding Author

*E-mail: julianne.gibbs@ualberta.ca

Notes

The authors declare no competing financial interest.

ACKNOWLEDGEMENT

J.M.G. gratefully acknowledges the Natural Sciences and Engineering Research Council of Canada for an Accelerator Award, the Alfred P. Sloan Foundation for a Research Fellowship, and Petro-Canada for a Young Innovator Award. B.R. gratefully acknowledges support from the Alberta/Technical University of Munich International Graduate School for Hybrid Functional

Materials (ATUMS-NSERC CREATE) program, the University of Alberta Future Energy Systems, and the Queen Elizabeth II Graduate Scholarship. B.R. and T.A.J. gratefully acknowledge the Natural Sciences and Engineering Research Council of Canada for a Canada Graduate Scholarship. Molecular dynamics simulations were run on WestGrid clusters. Belaid Moa (University of Victoria, WestGrid, Compute Canada) provided valuable assistance with the resource allocation and troubleshooting to run our simulations.

References:

1. Shen, Y. R., *The Principles of Nonlinear Optics*. New York: J. Wiley: 1984.
2. Shen, Y. R., Surface Properties Probed by Second-Harmonic and Sum-Frequency Generation. *Nature* **1989,** *337*, 519-525.
3. Shen, Y. R., Optical Second Harmonic Generation at Interfaces. *Annu. Rev. Phys. Chem.* **1989,** *40* (1), 327-350.
4. Shen, Y. R., *Fundamentals of Sum-Frequency Spectroscopy*. Cambridge University Press: Cambridge, 2016.
5. Shen, Y. R.; Ostroverkhov, V., Sum-Frequency Vibrational Spectroscopy on Water Interfaces: Polar Orientation of Water Molecules at Interfaces. *Chem. Rev.* **2006,** *106*, 1140-1154.
6. Covert, P. A.; Hore, D. K., Geochemical Insight from Nonlinear Optical Studies of Mineral–Water Interfaces. *Annu. Rev. Phys. Chem.* **2016,** *67* (1), 233-257.
7. Geiger, F. M., Second Harmonic Generation, Sum Frequency Generation, and $\chi^{(3)}$: Dissecting Environmental Interfaces with a Nonlinear Optical Swiss Army Knife. *Annu. Rev. Phys. Chem.* **2009,** *60*, 61-83.
8. Eisenthal, K. B., Liquid Interfaces Probed by Second-Harmonic and Sum-Frequency Spectroscopy. *Chem. Rev.* **1996,** *96*, 1343-1360.
9. Li, I.; Bandara, J.; Shultz, M. J., Time Evolution Studies of the H_2O/Quartz Interface Using Sum Frequency Generation, Atomic Force Microscopy, and Molecular Dynamics. *Langmuir* **2004,** *20* (24), 10474-10480.
10. Iler, R. K., *The Chemistry of Silica: Solubility, Polymerization, Colloid and Surface Properties, and Biochemistry*. New York: Wiley: 1979.
11. Azam, M. S.; Weeraman, C. N.; Gibbs-Davis, J. M., Specific Cation Effects on the Bimodal Acid–Base Behavior of the Silica/Water Interface. *J. Phys. Chem. Lett.* **2012,** *3* (10), 1269-1274.
12. Azam, M. S.; Weeraman, C. N.; Gibbs-Davis, J. M., Halide-Induced Cooperative Acid–Base Behavior at a Negatively Charged Interface. *J. Phys. Chem. C* **2013,** *117* (17), 8840-8850.
13. Azam, M. S.; Darlington, A.; Gibbs-Davis, J. M., The Influence of Concentration on Specific Ion Effects at the Silica/Water Interface. *J. Phys. Condens. Mat.* **2014,** *26* (24), 244107.
14. DeWalt-Kerian, E. L.; Kim, S.; Azam, M. S.; Zeng, H.; Liu, Q.; Gibbs, J. M., pH-Dependent Inversion of Hofmeister Trends in the Water Structure of the Electrical Double Layer. *J. Phys. Chem. Lett.* **2017,** *8*, 2855-2861.
15. Jena, K. C.; Hore, D. K., Variation of Ionic Strength Reveals the Interfacial Water Structure at a Charged Mineral Surface. *J. Phys. Chem. C* **2009,** *113* (34), 15364-15372.

16. Jena, K. C.; Covert, P. A.; Hore, D. K., The Effect of Salt on the Water Structure at a Charged Solid Surface: Differentiating Second- and Third-order Nonlinear Contributions. *J. Phys. Chem. Lett.* **2011,** *2*, 1056-1061.
17. Covert, P. A.; Jena, K. C.; Hore, D. K., Throwing Salt into the Mix: Altering Interfacial Water Structure by Electrolyte Addition. *J. Phys. Chem. Lett.* **2014,** *5*, 143-148.
18. Yang, Z.; Li, Q.; Chou, K. C., Structures of Water Molecules at the Interfaces of Aqueous Salt Solutions and Silica:Cation Effects. *J. Phys. Chem. C* **2009,** *113*, 8201-8205.
19. Lovering, K. A.; Bertram, A. K.; Chou, K. C., New Information on the Ion-Identity-Dependent Structure of Stern Layer Revealed by Sum Frequency Generation Vibrational Spectroscopy. *J. Phys. Chem. C* **2016,** *120* (32), 18099-18104.
20. Flores, S. C.; Kherb, J.; Cremer, P. S., Direct and Reverse Hofmeister Effects on Interfacial Water Structure. *J. Phys. Chem. C* **2012,** *116* (27), 14408-14413.
21. Flores, S. C.; Kherb, J.; Konelick, N.; Chen, X.; Cremer, P. S., The Effects of Hofmeister Cations at Negatively Charged Hydrophilic Surfaces. *J. Phys. Chem. C* **2012,** *116* (9), 5730-5734.
22. Ong, S.; Zhao, X.; Eisenthal, K. B., Polarization of Water Molecules at a Charged Interface: Second Harmonic Studies of the Silica/Water Interface. *Chem. Phys. Lett.* **1992,** *191* (3–4), 327-335.
23. Du, Q.; Freysz, E.; Shen, Y. R., Vibrational Spectra of Water Molecules at Quartz/Water Interfaces. *Phys. Rev. Lett.* **1994,** *72* (2), 238-241.
24. Campen, R. K.; Pymer, A. K.; Nihonyanagi, S.; Borguet, E., Linking Surface Potential and Deprotonation in Nanoporous Silica: Second Harmonic Generation and Acid/Base Titration. *J. Phys. Chem. C* **2010,** *114* (43), 18465-18473.
25. Ostroverkhov, V.; Waychunas, G. A.; Shen, Y. R., Vibrational Spectra of Water at Water/α-Quartz (0001) Interface. *Chem. Phys. Lett.* **2004,** *386* (1–3), 144-148.
26. Ostroverkhov, V.; Waychunas, G. A.; Shen, Y. R., New Information on Water Interfacial Structure Revealed by Phase-Sensitive Surface Spectroscopy. *Phys. Rev. Lett.* **2005,** *94* (4), 046102.
27. Dewan, S.; Yeganeh, M. S.; Borguet, E., Experimental Correlation Between Interfacial Water Structure and Mineral Reactivity. *J. Phys. Chem. Lett.* **2013,** *4*, 1977-1982.
28. Dalstein, L.; Potapova, E.; Tyrode, E., The Elusive Silica/Water Interface: Isolated Silanols Under Water as Revealed by Vibrational Sum Frequency Spectroscopy. *Phys. Chem. Chem. Phys.* **2017,** *19*, 10343-10349.
29. Ohno, P. E.; Wang, H.-f.; Geiger, F. M., Second-Order Spectral Lineshapes from Charged Interfaces. *Nat. Commun.* **2017,** *8* (1), 1032.
30. Boamah, M. D.; Ohno, P. E.; Geiger, F. M.; Eisenthal, K. B., Relative Permittivity in the Electrical Double Layer from Nonlinear Optics. *J. Chem. Phys.* **2018,** *148* (22), 222808.
31. Ohno, P. E.; Wang, H.-f.; Paesani, F.; Skinner, J. L.; Geiger, F. M., Second-Order Vibrational Lineshapes from the Air/Water Interface. *J. Phys. Chem. A* **2018,** *122* (18), 4457-4464.
32. Schaefer, J.; Gonella, G.; Bonn, M.; Backus, E. H. G., Surface-Specific Vibrational Spectroscopy of the Water/Silica Interface: Screening and Interference. *Phys. Chem. Chem. Phys.* **2017,** *19* (25), 16875-16880.
33. Wen, Y.-C.; Zha, S.; Liu, X.; Yang, S.; Guo, P.; Shi, G.; Fang, H.; Shen, Y. R.; Tian, C., Unveiling Microscopic Structures of Charged Water Interfaces by Surface-Specific Vibrational Spectroscopy. *Phys. Rev. Lett.* **2016,** *116* (1), 016101.
34. Gonella, G.; Lütgebaucks, C.; de Beer, A. G. F.; Roke, S., Second Harmonic and Sum-Frequency Generation from Aqueous Interfaces Is Modulated by Interference. *J. Phys. Chem. C* **2016,** *120* (17), 9165-9173.
35. Ohno, P. E.; Saslow, S. A.; Wang, H.-f.; Geiger, F. M.; Eisenthal, K. B., Phase-Referenced Nonlinear Spectroscopy of the α-Quartz/Water Interface. *Nat. Commun.* **2016,** *7*, 13587.

36. Konek, C. T.; Musorrafiti, M. J.; Al-Abadleh, H. A.; Bertin, P. A.; Nguyen, S. T.; Geiger, F. M., Interfacial Acidities, Charge Densities, Potentials, and Energies of Carboxylic Acid-Functionalized Silica/Water Interfaces Determined by Second Harmonic Generation. *J. Am. Chem. Soc.* **2004,** *126* (38), 11754-11755.
37. Gibbs-Davis, J. M.; Kruk, J. J.; Konek, C. T.; Scheidt, K. A.; Geiger, F. M., Jammed Acid−Base Reactions at Interfaces. *J. Am. Chem. Soc.* **2008,** *130* (46), 15444-15447.
38. Lützenkirchen, J.; Scharnweber, T.; Ho, T.; Striolo, A.; Sulpizi, M.; Abdelmonem, A., A Set-Up for Simultaneous Measurement of Second Harmonic Generation and Streaming Potential and Some Test Applications. *J. Colloid Interf. Sci.* **2018,** *529*, 294-305.
39. Malin, J. N.; Holland, J. G.; Saslow, S. A.; Geiger, F. M., U(VI) Adsorption and Speciation at the Acidic Silica/Water Interface Studied by Resonant and Nonresonant Second Harmonic Generation. *J. Phys. Chem. C* **2011,** *115* (27), 13353-13360.
40. Fitts, J. P.; Shang, X.; Flynn, G. W.; Heinz, T. F.; Eisenthal, K. B., Electrostatic Surface Charge at Aqueous/α-Al_2O_3 Single-Crystal Interfaces as Probed by Optical Second-Harmonic Generation. *J. Phys. Chem. B* **2005,** *109* (16), 7981-7986.
41. Stack, A. G.; Higgins, S. R.; Eggleston, C. M., Point of Zero Charge of a Corundum-Water Interface Probed with Optical Second Harmonic Generation (SHG) And Atomic Force Microscopy (AFM): New Approaches to Oxide Surface Charge. *Geochim. Cosmochim. Ac.* **2001,** *65* (18), 3055-3063.
42. Fitts, J. P.; Machesky, M. L.; Wesolowski, D. J.; Shang, X.; Kubicki, J. D.; Flynn, G. W.; Heinz, T. F.; Eisenthal, K. B., Second-Harmonic Generation and Theoretical Studies of Protonation at the Water/α-TiO_2 (1 1 0) Interface. *Chem. Phys. Lett.* **2005,** *411* (4–6), 399-403.
43. de Beer, A. G. F.; Campen, R. K.; Roke, S., Separating Surface Structure and Surface Charge with Second-Harmonic and Sum-Frequency Scattering. *Phys. Rev. B* **2010,** *82* (23), 235431.
44. Gragson, D. E.; McCarty, B. M.; Richmond, G. L., Ordering of Interfacial Water Molecules at the Charged Air/Water Interface Observed by Vibrational Sum Frequency Generation. *J. Am. Chem. Soc.* **1997,** *119* (26), 6144-6152.
45. Gragson, D. E.; Richmond, G. L., Potential Dependent Alignment and Hydrogen Bonding of Water Molecules at Charged Air/Water and CCl_4/Water Interfaces. *J. Am. Chem. Soc.* **1998,** *120* (2), 366-375.
46. Gragson, D. E.; Richmond, G. L., Investigations of the Structure and Hydrogen Bonding of Water Molecules at Liquid Surfaces by Vibrational Sum Frequency Spectroscopy. *J. Phys. Chem. B* **1998,** *102* (20), 3847-3861.
47. Joutsuka, T.; Hirano, T.; Sprik, M.; Morita, A., Effects of Third-Order Susceptibility in Sum Frequency Generation Spectra: A Molecular Dynamics Study in Liquid Water. *Phys. Chem. Chem. Phys.* **2018,** *20* (5), 3040-3053.
48. Darlington, A. M.; Jarisz, T. A.; DeWalt-Kerian, E. L.; Roy, S.; Kim, S.; Azam, M. S.; Hore, D. K.; Gibbs, J. M., Separating the pH-Dependent Behavior of Water in the Stern and Diffuse Layers with Varying Salt Concentration. *J. Phys. Chem. C* **2017,** *121* (37), 20229-20241.
49. Darlington, A. M.; Gibbs-Davis, J. M., Bimodal or Trimodal? The Influence of Starting pH on Site Identity and Distribution at the Low Salt Aqueous/Silica Interface. *J. Phys. Chem. C* **2015,** *119* (29), 16560-16567.
50. Yeganeh, M. S.; Dougal, S. M.; Pink, H. S., Vibrational Spectroscopy of Water at Liquid/Solid Interfaces: Crossing the Isoelectric Point of a Solid Surface. *Phys. Rev. Lett.* **1999,** *83* (6), 1179-1182.
51. Sung, J.; Zhang, L.; Tian, C.; Shen, Y. R.; Waychunas, G. A., Effect of pH on the Water/α-Al_2O_3 ($1\bar{1}02$) Interface Structure Studied by Sum-Frequency Vibrational Spectroscopy. *J. Phys. Chem. C* **2011,** *115* (28), 13887-13893.
52. Kataoka, S.; Gurau, M. C.; Albertorio, F.; Holden, M. A.; Lim, S.-M.; Yang, R. D.; Cremer, P. S., Investigation of Water Structure at the TiO_2/Aqueous Interface. *Langmuir* **2004,** *20* (5), 1662-1666.

53. Zhao, X.; Ong, S.; Eisenthal, K. B., Polarization of Water Molecules at a Charged Interface. Second Harmonic Studies of Charged Monolayers at the Air/Water Interface. *Chem. Phys. Lett.* **1993,** *202* (6), 513-520.
54. Dreier, L. B.; Bernhard, C.; Gonella, G.; Backus, E. H. G.; Bonn, M., Surface Potential of a Planar Charged Lipid–Water Interface. What Do Vibrating Plate Methods, Second Harmonic and Sum Frequency Measure? *J. Phys. Chem. Lett.* **2018,** *9* (19), 5685-5691.
55. Sauerbeck, C.; Braunschweig, B.; Peukert, W., Surface Charging and Interfacial Water Structure of Amphoteric Colloidal Particles. *J. Phys. Chem. C* **2014,** *118* (19), 10033-10042.
56. Roy, S.; Hore, D. K., Simulated Structure and Nonlinear Vibrational Spectra of Water Next to Hydrophobic and Hydrophilic Solid Surfaces. *J. Phys. Chem. C* **2012,** *116* (43), 22867-22877.
57. Morita, A.; Hynes, J. T., A Theoretical Analysis of the Sum Frequency Generation Spectrum of the Water Surface. *Chem. Phys.* **2000,** *258* (2), 371-390.
58. Kitamura, A.; Fujiwara, K.; Yamamoto, T.; Nishikawa, S.; Moriyama, H., Analysis of Adsorption Behavior of Cations onto Quartz Surface by Electrical Double-layer Model. *J. Nucl. Sci. Technol.* **1999,** *36* (12), 1167-1175.
59. Icenhower, J. P.; Dove, P. M., The Dissolution Kinetics of Amorphous Silica into Sodium Chloride Solutions: Effects of Temperature and Ionic Strength. *Geochim. Cosmochim. Ac.* **2000,** *64* (24), 4193-4203.
60. Grahame, D. C., The Electrical Double Layer and the Theory of Electrocapillarity. *Chem. Rev.* **1947,** *41* (3), 441-501.
61. Smith, A. M.; Lee, A. A.; Perkin, S., The Electrostatic Screening Length in Concentrated Electrolytes Increases with Concentration. *J. Phys. Chem. Lett.* **2016,** *7* (12), 2157-2163.
62. Pezzotti, S.; Galimberti, D. R.; Shen, Y. R.; Gaigeot, M.-P., Structural Definition of the BIL and DL: A New Universal methodology to Rationalize Non-Linear $\chi^{(2)}(\omega)$ SFG Signals at Charged Interfaces, Including $\chi^{(3)}(\omega)$ Contributions. *Phys. Chem. Chem. Phys* **2018,** *20* (7), 5190-5199.
63. Myalitsin, A.; Urashima, S.; Nihonyanagi, S.; Yamaguchi, S.; Tahara, T., Water Structure at the Buried Silica/Aqueous Interface Studied by Heterodyne-Detected Vibrational Sum-Frequency Generation. *J. Phys. Chem. C* **2016,** *120* (17), 9357-9363.
64. Zhang, H.; Hassanali, A. A.; Shin, Y. K.; Knight, C.; Singer, S. J., The Water–Amorphous Silica Interface: Analysis of the Stern Layer and Surface Conduction. *J. Chem. Phys.* **2011,** *134* (2), 024705.
65. Hartkamp, R.; Siboulet, B.; Dufrêche, J.-F.; Coasne, B., Ion-Specific Adsorption and Electroosmosis in Charged Amorphous Porous Silica. *Phys. Chem. Chem. Phys.* **2015,** *17* (38), 24683-24695.
66. Haria, N. R.; Lorenz, C. D., Atomistic Description of Pressure-Driven Flow of Aqueous Salt Solutions through Charged Silica Nanopores. *J. Phys. Chem. C* **2015,** *119* (22), 12298-12311.
67. Roy, S.; Naka, T. L.; Hore, D. K., Enhanced Understanding of Amphipathic Peptide Adsorbed Structure by Modeling of the Nonlinear Vibrational Response. *J. Phys. Chem. C* **2013,** *117* (47), 24955-24966.
68. Zhang, L.; Singh, S.; Tian, C.; Shen, Y. R.; Wu, Y.; Shannon, M. A.; Brinker, C. J., Nanoporous Silica-Water Interfaces Studied by Sum-Frequency Vibrational Spectroscopy. *J. Chem. Phys.* **2009,** *130* (15), 154702.
69. Urashima, S.-h.; Myalitsin, A.; Nihonyanagi, S.; Tahara, T., The Topmost Water Structure at a Charged Silica/Aqueous Interface Revealed by Heterodyne-Detected Vibrational Sum Frequency Generation Spectroscopy. *J. Phys. Chem. Lett.* **2018,** *9* (14), 4109-4114.

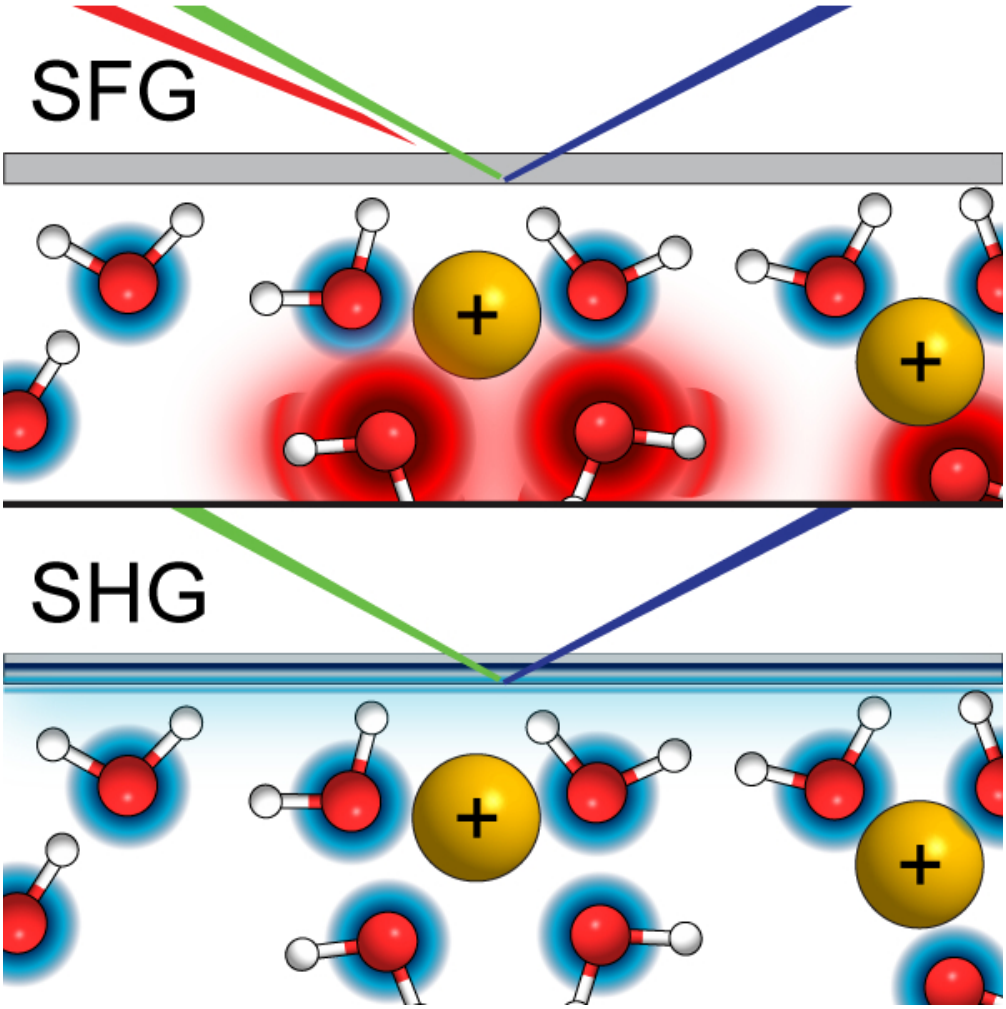
SFG
SHG

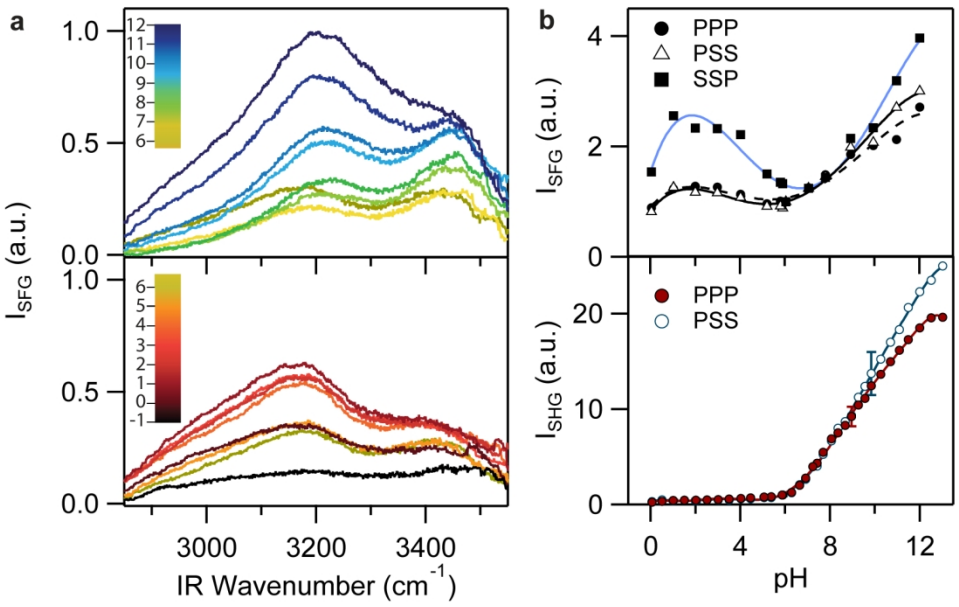

Figure 1. a) ssp-SFG spectra from 2850 – 3550 cm^{-1} measured at the silica/water interface at 500 mM NaCl over a pH range of 5.8 to 12 (top panel) and 5.8 to below 0 (bottom panel). SFG spectra are corrected for local field effects and normalized to maximum intensity at high pH. b) Integrated SFG intensities at the ssp, pss, and ppp polarization combinations (top) and the SHG intensity at the p-in/p-out (ppp) and s-in/p-out (pss) polarization combinations over the pH range studied. Integrated SFG intensities and SHG intensities are normalized to their values at pH 6. Smooth lines are guides for the eye.

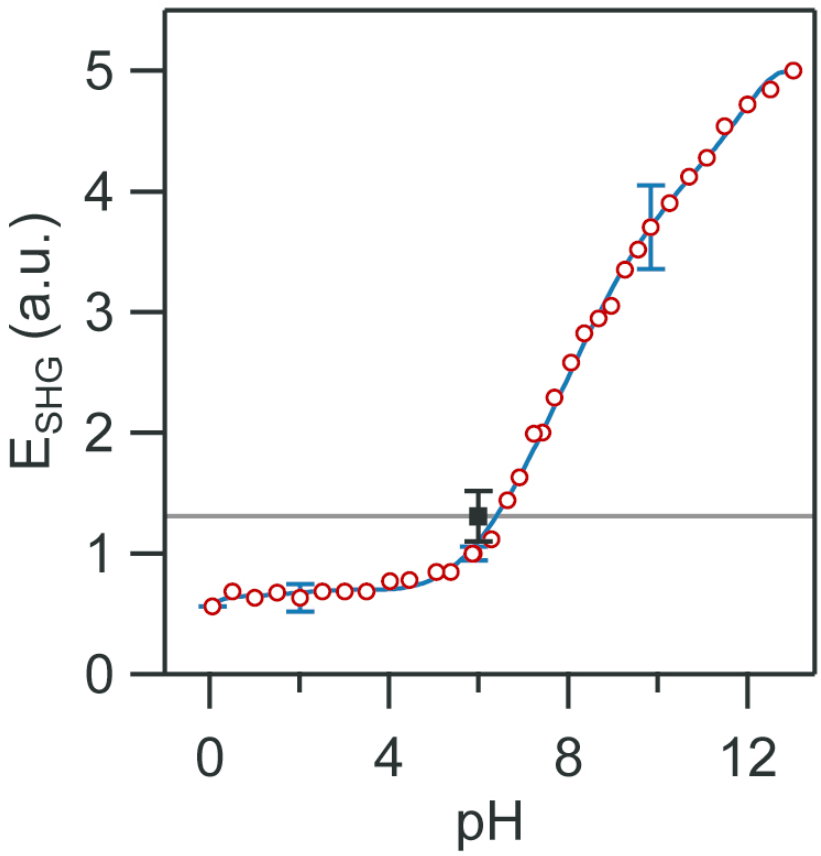

Figure 2. Comparison of pss-SHG electric field at the silica/water interface (500 mM NaCl, circles) to the pss-SHG electric field at the silica/air interface (square and horizontal line). Error bars represent the standard deviation between multiple experiments. The smooth line is a guide for the eye.

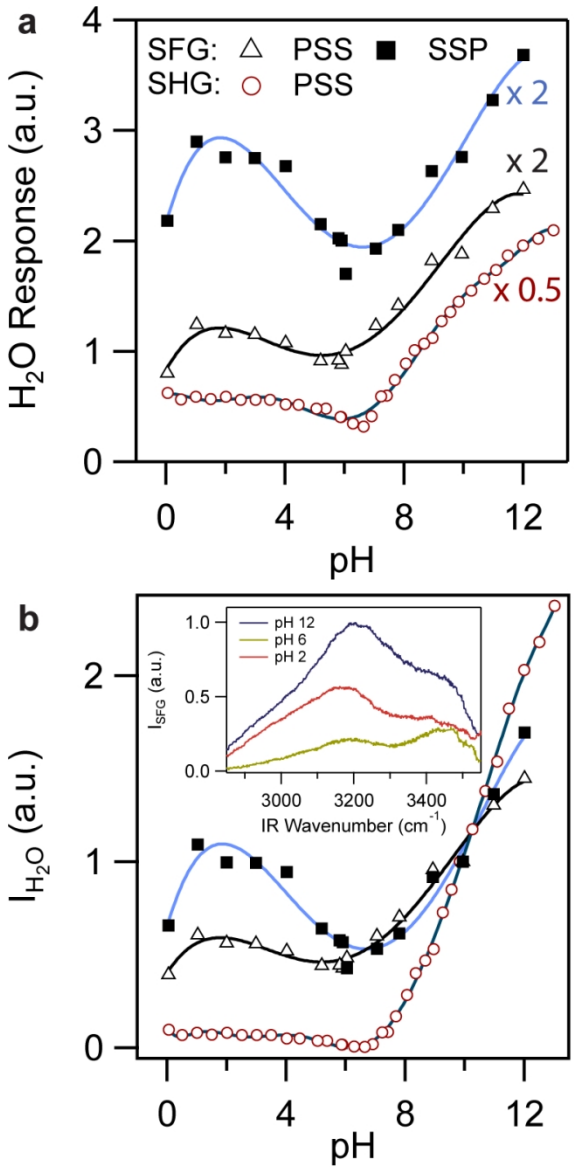

Figure 3. a) The water response proportional to $|\chi^{(2)}_{H2O}+\chi^{(3)}_{H2O}\Phi_0|$ calculated from SHG and integrated SFG. Data are offset and multiplied for clarity. b) The integrated SFG intensities compared to the square of the second harmonic water response. Intensities are normalized to their values at pH 10. (inset: SFG spectra at the silica/aqueous sodium chloride interface at pH 12, 6, and 2. Smooth lines are guides for the eye).

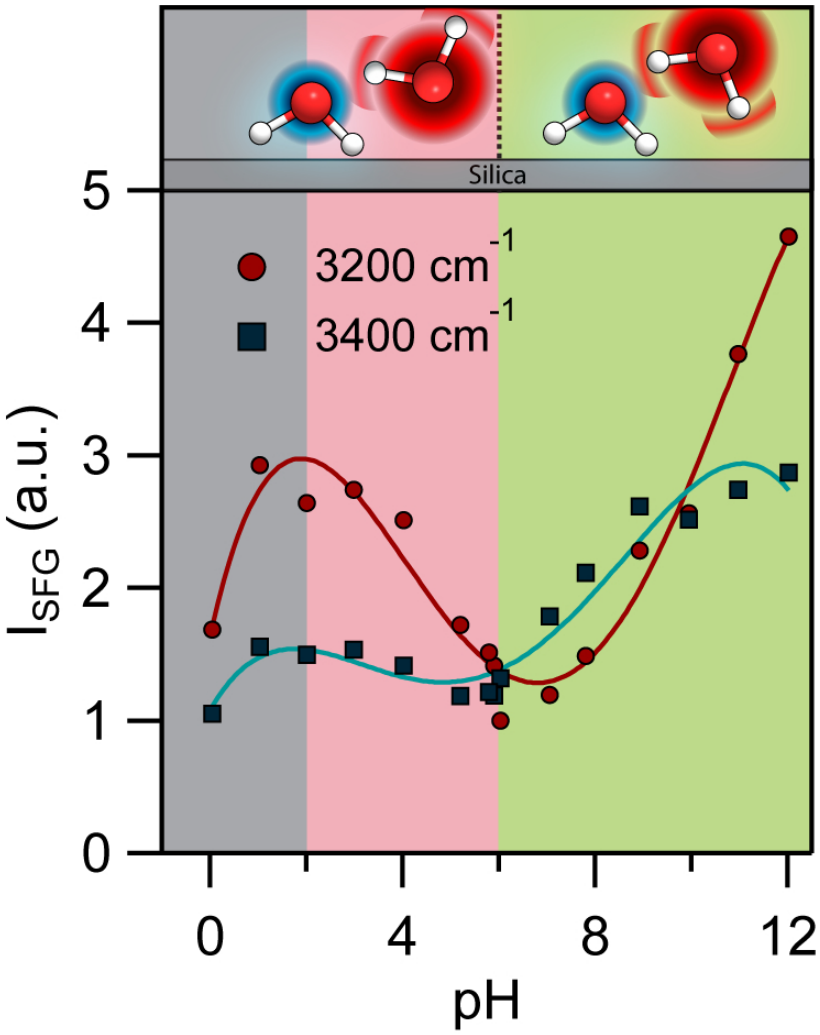

Figure 4. Intensities of ssp-SFG at a) 3185 cm^{-1} and b) 3455 cm^{-1}. Intensities are normalized to the 3185 cm^{-1} values at pH 6. Green and red shading indicate possible constructive and destructive interference between water populations, respectively. Smooth lines are guides for the eye. Top: Illustration of flipping water molecules contributing to the low wavenumber region.

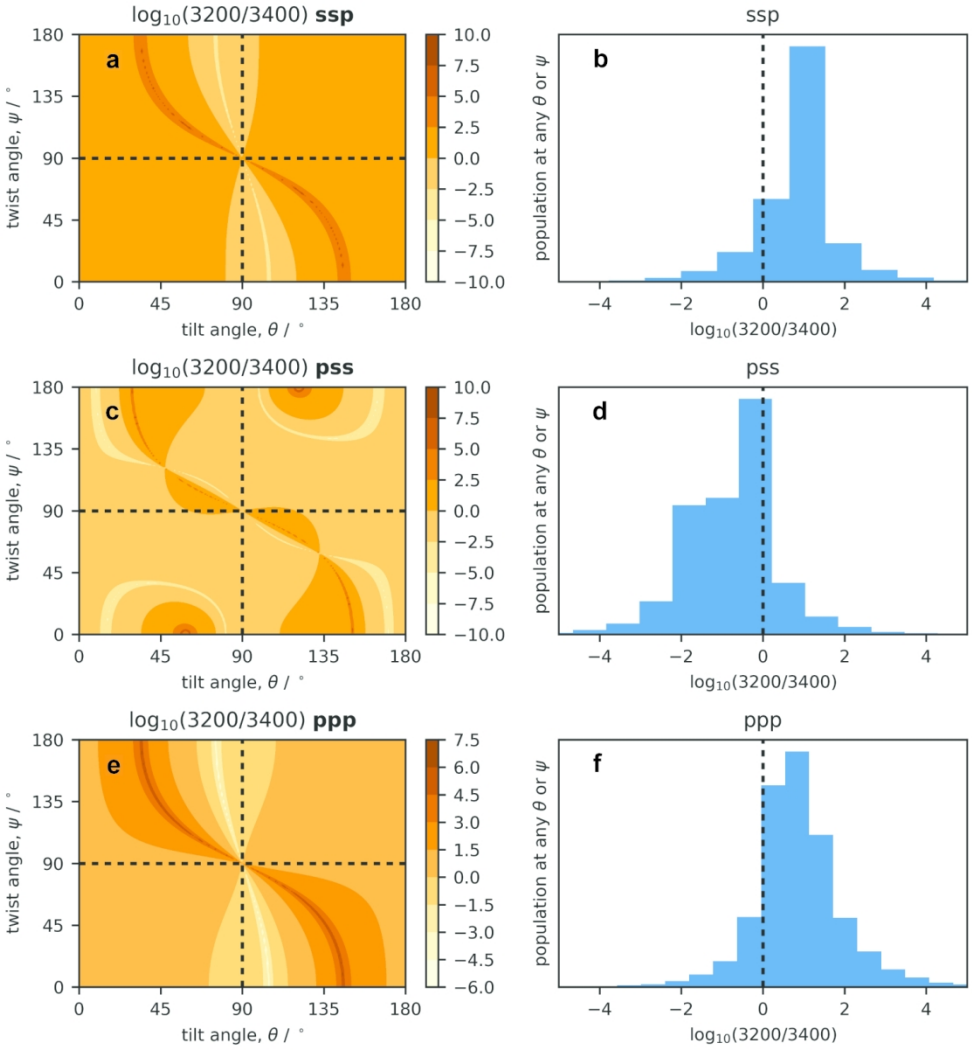

Figure 5. Log ratios of β_{3200} and β_{3400} at all possible twist and tilt angles calculated for the A) ssp, C) pss and E) ppp polarization combinations. Histograms of the frequency that each log ratio value occurred in the corresponding twist and tilt maps are shown for the B) ssp, D) pss and F) ppp polarization combinations.